Journal of Hydrology 556 (2018) 523–538

Contents lists available at ScienceDirect

Journal of Hydrology

journal homepage: www.elsevier.com/locate/jhydrol

Research papers

Analyzing climate change impacts on water resources under uncertainty using an integrated simulation-optimization approach

X.W. Zhuang [a,b], Y.P. Li [c,*], S. Nie [d], Y.R. Fan [e], G.H. Huang [e]

[a] Institute for Civil Engineering, Qingdao Huanghai University, Qingdao 266427, China
[b] Sino-Canada Resources and Environmental Research Center, North China Electric Power University, Beijing 102206, China
[c] State Key Laboratory of Water Environment Simulation, School of Environment, Beijing Normal University, Beijing 100875, China
[d] Faculty of Applied Science and Engineering, University of Toronto, Toronto, ON M5S 1A4, Canada
[e] Institute for Energy, Environment and Sustainable Communities, University of Regina, Regina, Saskatchewan S4S 0A2, Canada

ARTICLE INFO

Article history:
Received 14 May 2017
Received in revised form 6 November 2017
Accepted 9 November 2017
Available online 14 November 2017
This manuscript was handled by Marco Borga, Editor-in-Chief, with the assistance of Ashish Sharma, Associate Editor

Keywords:
Climate change
Multistage
Simulation-optimization
Stochastic analysis
Uncertainty
Water resources

ABSTRACT

An integrated simulation-optimization (ISO) approach is developed for assessing climate change impacts on water resources. In the ISO, uncertainties presented as both interval numbers and probability distributions can be reflected. Moreover, ISO permits in-depth analyses of various policy scenarios that are associated with different levels of economic consequences when the promised water-allocation targets are violated. A snowmelt-precipitation-driven watershed (Kaidu watershed) in northwest China is selected as the study case for demonstrating the applicability of the proposed method. Results of meteorological projections disclose that the incremental trend of temperature (e.g., minimum and maximum values) and precipitation exist. Results also reveal that (i) the system uncertainties would significantly affect water resources allocation pattern (including target and shortage); (ii) water shortage would be enhanced from 2016 to 2070; and (iii) the more the inflow amount decreases, the higher estimated water shortage rates are. The ISO method is useful for evaluating climate change impacts within a watershed system with complicated uncertainties and helping identify appropriate water resources management strategies hedging against drought.

1. Introduction

Global warming has measurable effects on a hydrological cycle, altering the amount, distribution and timing of available water (Kandiah et al., 2016). Climate change affects water supply through hydrologic extreme, which potentially results in flooding and drought risks (Poorsepahy-Samian et al., 2016). Increasing water demand with socioeconomic development and population growth as well as shrinking water availability due to climatic and anthropogenic changes has brought conflict-laden issues of water resources allocation (Andersson et al., 2006). Water resources management has become a challenging task under changing climate. Therefore, forecast of climate change scenarios and assessment of its impacts on water resources can help decision makers implement mitigating policies and make strategic investment in infrastructure for future water resources management (Rheinheimer et al., 2016). However, the impacts of climate change are difficult to investigate due to uncertainties of meteorological projection as well as the inherent nonlinearity and complexity of climate-hydrological processes; besides, in real-world problems, many parameters in water resources systems are highly uncertain and their interrelationships could be extremely complicated (Li and Huang, 2009; Wasko and Sharma, 2016).

Previously, a number of research efforts were conducted to cope with uncertainties in simulation and optimization of water resources systems (Li et al., 2009a). Due to a variety of uncertainties existed in hydrological model structure and forecasting capability, more and more literatures investigated uncertainties in hydrological processes. Besides, uncertain factors (e.g., climate change) impacts on variability of water resources exist in management models (Nguyen et al., 2016). For instance, Watkins et al. (2000) proposed a scenario-based multistage stochastic programming model for planning water supplies from highland lakes, where dynamics and uncertainties of water availability (and thus water allocation) could be taken into account through generation of multiple representative scenarios. Jiang et al. (2007) used six conceptual rainfall-runoff models to examine hydrological model structure uncertainties under fifteen hypothetical climate change scenarios (from the combinations of three temperature increases

* Corresponding author.
E-mail address: yongping.li@iseis.org (Y.P. Li).

https://doi.org/10.1016/j.jhydrol.2017.11.016
0022-1694/

and five precipitation changes). Li et al. (2009b) studied an agricultural catchment area on the Loess Plateau in China during the period 1981–2000 and identified the separate impacts of climate change and land use/cover change on decreasing river flow amounting to about 95.8% and 9.6%, respectively. Poulin et al. (2011) employed two different simulation tools (lumped conceptual model and spatially-distributed physically-based model) to investigate the effects of model structure and parameter equifinality on the uncertainty related to hydrological modelling in climate impact studies. Wada et al. (2013) used seven global hydrological models to quantify the impact of projected global climate change on future water demand; results indicate that uncertainties arising from hydrological models and global climate models (GCMs) are large. Borgomeo et al. (2014) proposed nonstationary synthetic time series of future climates obtained via a stochastic weather generator to construct a probability distribution of the frequency of future water shortages, and provided the basis for testing the robustness of water resources management to future climate-related uncertainties. Kotir et al. (2016) developed an integrated dynamics simulation model to examine the feedback processes and interaction among population, water resource and agricultural production sub-sectors; results show that the model is reliable and robust to uncertainties in model structure, parameters and inputs. As mentioned above, despite the levels of uncertainty associated with the magnitude and direction of climate variability and change, they are expected to have impacts on water availability. The effects of climate change on the hydrological cycle include variations in the quantity and seasonal distribution of precipitation, increased precipitation intensity, increasingly frequent and severe temperature fluctuations and weather events, as well as redistributed balance between rain and snow. There is much heterogeneity in the climate change models used as well as the assumptions made.

A tendency of increment in runoff has been observed in northwestern China, which is supplied by melting ice, snowmelt and precipitation. Future changes in hydrological processes and stream flows have become increasingly essential to water resources management in the northwest of China. With the climate change anticipated to have threatening consequences on water resources and environment both at the global level and at local/regional levels (e.g., increases in the number and magnitude of floods and droughts, increases in sea levels), a general assessment is that the future state of water will be a lot worse than it is now (UNESCO, 2002; Lobell et al., 2011). Besides, the lack of understanding of climate dynamics, as well as various uncertainties associated with future emission scenarios and their spatial and temporal details, hinder the capability to provide reliable climate change scenarios. Nevertheless, various complexities and uncertainties existed in water resources systems, pose significant challenges to water resources planning and hydrologic prediction under changing climate (Fan et al., 2016). Water resources management under changing climate is complicated due to (i) the disagreement among climate change scenarios, (ii) formulation of appropriate techniques for downscaling global climate model (GCM) outputs to local condition for hydrologic prediction, (iii) difference between simplification of hydrological model and nonlinearity of hydroprocessing, and (iv) error of water management planning or policy that should not be ignored in practical applications (Risbey, 1998). For example, water supply and demand can continue to change commensurate with changes in population, economic condition, social and political factors, as well as investment in supply systems (Harman et al., 2011). Besides, water management arises in the context of complex and interdependent ecological, social and economic systems, whose behavior is governed by numerous feedback interactions that are characterized by nonlinearity. Correspondingly, mitigation of adverse conditions and reliable estimation of the associated uncertainties inherent in water management under climate change is desirable (Consigli and Dempster, 1998). This brings a number of challenges to water-related professionals, policymakers, and stakeholders. It is desired that more innovative approaches are developed, with improved algorithms in propagating uncertainties associated with both climate changing modeling and hydrological analysis (Naadimuthu, 1982).

Therefore, the objective of this study is to develop an integrated simulation-optimization (ISO) method to evaluate climate change impacts on water resources, through incorporating techniques of multi-ensemble GCMs, daily climate-streamflow hydrological simulation, and interval-multistage chance-constrained (IMC) optimization into a general framework. ISO can not only address the model-related uncertainties in meteorological prediction, in hydrological simulation and in water resources allocation, but also examine the risk of violating individual probabilistic constraints under various scenarios. A case study of the Kaidu watershed in northwestern China will then be provided for demonstrating how the developed method will support water resources management under climate change.

2. Methodology

2.1. General framework of ISO

ISO is consisted of (i) climate projection from multi-ensemble GCMs, (ii) daily climate-streamflow hydrological simulation, and (iii) interval-multistage chance-constrained optimization. The general flow chart is shown in Fig. 1. First, the large-scale simulation outputs (e.g., minimum and maximum temperatures, precipitation) of multi-ensemble GCMs are downscaled for constructing watershed-scale meteorological scenarios. Second, the daily climate-streamflow hydrological simulation is employed to simulate streamflows in baseline (1961–1990), recent (2006–2011) and future (2016–2070) periods. Consequently, the downscaled meteorological projections are used as inputs into the hydrological simulation and, then, hydrologic model is used to simulate streamflows that are used as inputs into a water resources management model. Finally, IMC is used for optimizing water resources allocation under climate change and uncertainty. IMC can tackle random parameters in constraints and intervals in objective function as well as reflect risk of violating individual probabilistic constraints (Watkins et al., 2000; Li et al., 2006). The proposed ISO approach can thus examine various water-allocation patterns with different risks of violating water-demand targets, and further illustrate the individual probabilities of different combinations of water supply and water demand quantitatively (Zarghami and Akbariyeh, 2012).

2.2. Climate change projections

Datasets of observed and simulated meteorological variables are collected for watershed climate change impact analysis. The historical datasets of meteorological variables (precipitation and minimum/maximum temperatures) during the period of 1961–2011 in the Kaidu watershed are obtained from three meteorological stations (i.e., Baluntai, Bayinbuluke and Yanqi). The Dashankou hydrological station provides dataset of daily streamflow ranging from 1957 to 2011. Besides, GCM is an effective tool for simulating/predicting climate. However, climate scenarios calculated by GCMs are subject to significant uncertainties in particular regarding precipitation. Because single model is overconfident and multi-model ensemble of GCMs contains information from all participating models, it is generally believed that multi-model ensemble is superior to single model (Wilby and Harris, 2006). Correspondingly, the dataset of average values calculated from

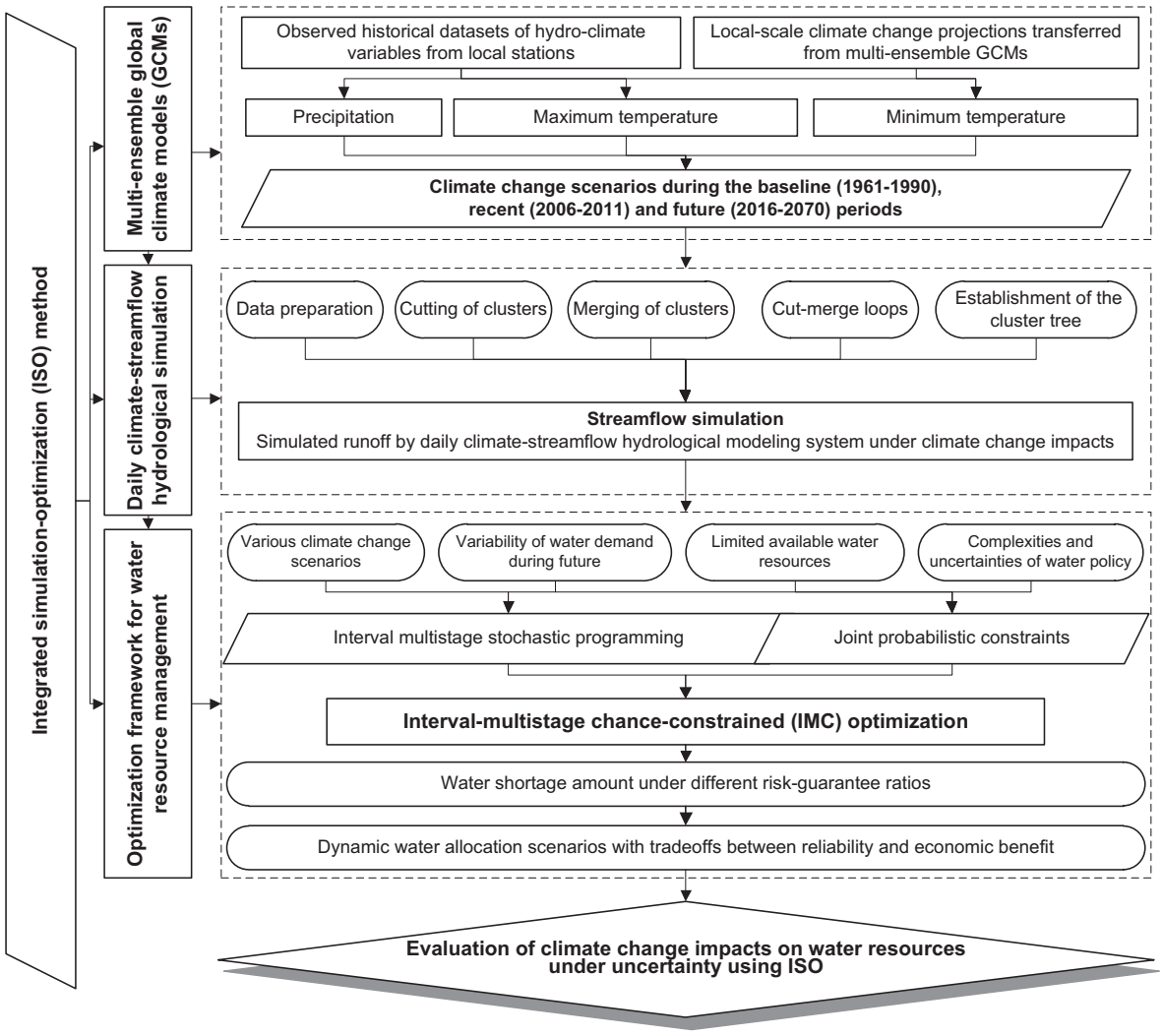

Fig. 1. Flow chart.

multi-ensemble GCMs is employed for meteorological projections, which allows ensemble climate projections to reduce the bias of simulated outputs (Woldemeskel et al., 2016). In this study, the simulated results under IPCC RCP4.5 scenario in baseline (1961–1990), recent (2006–2011) and future (2016–2070) periods are obtained from multi-ensemble GCMs (CCSM, HadCM3 and MRI-CGCM).

Uncertainties in climate change projections are derived from the difference of GCMs as well as the utilization of statistical downscaling tools (Milly et al., 2002). In fact, since GCMs produce outputs at much larger spatial scales than those required for catchment-scale hydrologic and water resources analyses, transformation of data among these scales (i.e., downscaling) becomes essential (Reshmidevi et al., 2018). In this study, the stepwise-clustered downscaling method is employed for atmospheric simulation outputs (predictors) to acquire high-resolution climate projections (predictands) with discrete and nonlinear uncertainties (Sharma et al., 2012; Wang et al., 2013; Zhuang et al., 2016a). In detail, the simulation outputs are effectively extracted from multi-ensemble GCMs to reduce the uncertain effect of climate projection and, then, the large-scale climate projections are transferred by the statistical downscaling method to construct watershed-scale meteorological simulations (e.g., daily maximum/minimum temperature and precipitation) (Zhuang et al., 2016a).

2.3. Hydrological simulation

Through using observed and downscaled climate variables (maximum and minimum temperatures, precipitation) as inputs, a daily climate-streamflow hydrological simulation based on stepwise cluster analysis (SCA) technique is employed for streamflows simulation in the Kaidu watershed (Zhuang et al., 2016b). The detailed steps include (1) data preparation of system inputs and outputs, which generally requires some necessary correlation analyses for each pair of inputs and outputs, (2) cutting of clusters based on clustering principles, (3) merging of clusters, (4) cut-merge loops, (5) establishment of the cluster tree, and (6) generation of required streamflow. When a new sample ($x_1, x_2, \ldots, x_m, y$; y is unknown) enters the tree at a cutting point, the sample will finally drop into a tip cluster which cannot be either cut or merged further according to the routes decided by new independent variables ($x_1, x_2, \ldots, x_m$). The predicted value of y will be the mean of dependent variables of the training samples in the tip cluster. Thus, the SCA tree is capable of predicting new dependent variables when new samples enter the tree from top to bottom. The detailed interpretation for implementing SCA is provided in the Appendix A.

Datasets of hydro-meteorological variables (maximum and minimum temperatures, precipitation and streamflow) during 1961–1990 are used for calibration of the hydrological simulation, and datasets during 2006–2011 for verification. The simulated

results during calibration and validation are checked by Nash-sutcliffe efficiency (*NSE*) (Nash and Sutcliffe, 1970), and coefficient of correlation (R^2). The criteria are defined as follows:

$$NSE = 1 - \frac{\sum_{i=1}^{n}(obs_i - pred_i)^2}{\sum_{i=1}^{n}(obs_i - \overline{obs_i})^2} \tag{1a}$$

$$R^2 = \frac{(n\sum_{i=1}^{n} obs_i \cdot pred_i - \sum_{i=1}^{n} obs_i \cdot \sum_{i=1}^{n} pred_i)^2}{[n\sum_{i=1}^{n}(obs_i)^2 - (\sum_{i=1}^{n} obs_i)^2][n\sum_{i=1}^{n}(pred_i)^2 - (\sum_{i=1}^{n} pred_i)^2]} \tag{1b}$$

where obs_i is the observed data value on day i; $pred_i$ is the predicted data value on day i; and $\overline{obs_i}$ is the mean observed data value; n is the number of simulated days. The closer *NSE* and R^2 values to 1, the model performances are better.

2.4. Interval-multistage chance-constrained optimization

In this study, IMC method is proposed not only for dealing with uncertainties presented in terms of individual probabilities (i.e., a level of probability represents the admissible risk of violating the uncertain satisfactory constraints); but also for reflecting complexities in water allocation problems where interactive and dynamic relationships exist within a multistage context (Gulpinar et al., 2002). The techniques of chance-constrained programming (CCP) and multistage stochastic programming (MSP) are used for dealing with random uncertainties (Charnes et al., 1972; Li et al., 2006). Besides, uncertain parameters may be expressed as interval values with known lower and upper bounds, but unknown membership or distribution functions (Sun et al., 2013). For uncertainties in left-and right-hand sides and cost/revenue parameters in the objective function, an extended consideration is the introduction of techniques of interval-parameter programming (IPP) (Loukas et al., 2007). Thus, an interval-multistage chance-constrained (IMC) optimization approach is developed, through introduction of techniques of CCP, MSP and IPP into a general framework. Thus, we have:

$$Maxf^{\pm} = \sum_{t=1}^{T} C_t^{\pm} X_t^{\pm} - \sum_{t=1}^{T}\sum_{k=1}^{K_t} p_{tk} D_{tk}^{\pm} Y_{tk}^{\pm} \tag{2a}$$

subject to:

$$A_t^{\pm} X_{tk}^{\pm} \leqslant B_{th}^{\pm} \quad t = 1,2,\ldots,T \tag{2b}$$

$$A_t^{\pm} X_t^{\pm} + A_{tk}'^{\pm} Y_{tk}^{\pm} \leqslant \tilde{w}_{tk}^{\pm} \quad t = 1,2,\ldots,T;\ k = 1,2,\ldots,K_t \tag{2c}$$

$$\Pr\{(1+\theta_{st})A_{tk}^{\pm}(X_t^{\pm} - Y_{tk}^{\pm}) \leqslant B_{th}^{\pm}\} \geqslant 1 - q_s \quad s = 1,2,\ldots,m_3;\ t = 1,2,\ldots,T;\ k = 1,2,\ldots,K_t;\ h = 1,2,\ldots,H; \tag{2d}$$

$$\theta_{st} \hbar N(u_{st}, \sigma_{st}^2) \quad \forall s,t \tag{2e}$$

$$x_t^{\pm} \geqslant 0,\ x_t^{\pm} \in X_t^{\pm} \quad t = 1,2,\ldots,T \tag{2f}$$

$$y_{tk}^{\pm} \geqslant 0,\ y_{tk}^{\pm} \in Y_{tk}^{\pm} \quad t = 1,2,\ldots,T;\ k = 1,2,\ldots,K_t \tag{2g}$$

where superscripts '−' and '+' represent lower and upper bounds of the interval parameters, respectively. where $f^{\pm}$ is a linear objective function; $C_t^{\pm}$ are coefficients of first-stage variables $X_t^{\pm}$ in the objective function; $D_{tk}^{\pm}$ are coefficients of recourse variables $Y_{tk}^{\pm}$ in the objective function; $A_t^{\pm}$ and $B_{th}^{\pm}$ are real-number parameters; $X_t^{\pm}$ and $Y_{tk}^{\pm}$ are real-number decision variables, where those that must be determined before the realizations of random variables are disclosed (i.e., $X_t^{\pm}$), and those (recourse variables) that can be determined after the realized random variable values are available (i.e., $Y_{tk}^{\pm}$). where p_{tk} is probability of occurrence for scenario k in period t, with $p_{tk} > 0$ and $\sum_{k=1}^{K_t} p_{tk} = 1$; K_t is the number of scenarios in period t, and the total being $K = \sum_{t=1}^{T} K_t$; $\tilde{w}_{tk}^{\pm}$ is random variable of constraint t, which is associated with probability level p_{tk}; $Pr\{\hbar\}$ denotes the probability distribution function; t denotes the time period, $t = 1, 2,\ldots,T$; q_s ($s = 1, 2,\ldots, m_3$) are individual probabilities at which the entire set of uncertain constraints are enforced to be satisfied; θ_{st} are random parameters with normal distributions (u_{st} is expectation and σ_{st} is standard variation).

Model (2) is generally nonlinear and possibly non-convex due to the existence of joint probabilities for multiple random variables (θ_{st}). Correspondingly, a two-step solution method is proposed for solving model (2) (Li et al., 2006). The sub-model corresponding to f^+ can be formulated in the first step when the system objective is to be maximized; the other sub-model (corresponding to f^-) can then be formulated based on the solution of the first sub-model. Thus, the first sub-model is (assume that $B^{\pm} > 0$ and $f^{\pm} > 0$):

$$Maxf^{+} = \sum_{t=1}^{T}\left(\sum_{j=1}^{j_1} c_{jt}^{+} x_{jt}^{+} + \sum_{j=j_1+1}^{n_1} c_{jt}^{+} x_{jt}^{-}\right) - \sum_{t=1}^{T}\sum_{k=1}^{K_t} p_{tk}\left(\sum_{j=1}^{j_2} d_{jtk}^{-} y_{jtk}^{-} + \sum_{j=j_2+1}^{n_2} d_{jtk}^{-} y_{jtk}^{+}\right) \tag{3a}$$

subject to:

$$\sum_{j=1}^{j_1} |a_{rjt}|^{-}\mathrm{Sign}(a_{rjt}^{-}) x_{jt}^{+} + \sum_{j=j_1+1}^{n_1} |a_{rjt}|^{+}\mathrm{Sign}(a_{rjt}^{+}) x_{jt}^{-} \leqslant b_{rth}^{+} \quad \forall r,t,h \tag{3b}$$

$$\sum_{j=1}^{j_1} |a_{ijt}|^{-}\mathrm{Sign}(a_{ijt}^{-}) x_{jt}^{+} + \sum_{j=j_1+1}^{n_1} |a_{ijt}|^{+}\mathrm{Sign}(a_{ijt}^{+}) x_{jt}^{-} + \sum_{j=1}^{j_2} |a'_{ijtk}|^{+}\mathrm{Sign}(a'^{+}_{ijtk}) y_{jtk}^{-} + \sum_{j=j_2+1}^{n_2} |a'_{ijtk}|^{-}\mathrm{Sign}(a'^{-}_{ijt}) y_{jtk}^{+} \leqslant \tilde{w}_{itk}^{+} \quad \forall i,t;\ k = 1,2,\ldots,K_t \tag{3c}$$

$$\left[\sum_{j=1}^{j_1} |a_{sjt}|^{-}\mathrm{Sign}(a_{sjt}^{-}) x_{jt}^{+} + \sum_{j=j_1+1}^{n_1} |a_{sjt}|^{+}\mathrm{Sign}(a_{sjt}^{+}) x_{jt}^{-}\right] \times (u_{st} + \sigma_{st}\phi^{-1}(1-q_s)) \leqslant b_{sth}^{+} \quad \forall s,t,h \tag{3d}$$

$$x_{jt}^{+} \geqslant 0 \quad \forall t;\ j = 1,2,\ldots,j_1 \tag{3e}$$

$$x_{jt}^{-} \geqslant 0 \quad \forall t;\ j = j_1+1, j_1+2,\ldots,n_1 \tag{3f}$$

$$y_{jtk}^{-} \geqslant 0 \quad \forall t;\ j = 1,2,\ldots j_2;\ k = 1,2,\ldots,K_t \tag{3g}$$

$$y_{jtk}^{+} \geqslant 0 \quad \forall t;\ j = j_2+1, j_2+2,\ldots,n_2;\ k = 1,2,\ldots,K_t \tag{3h}$$

where $x_{jt}^{\pm}(j = 1,2,\ldots,j_1)$ are variables with positive coefficients in the objective function, $x_{jt}^{\pm}(j = j_1+1, j_1+2,\ldots,n_1)$ are variables with negative coefficients, $y_{jtk}^{\pm}(j = 1,2,\ldots,j_2$ and $k = 1,2,\ldots,K_t)$ are recourse variables with positive coefficients in the objective function, and $y_{jtk}^{\pm}(j = j_2+1, j_2+2,\ldots,n_2$ and $k = 1,2,\ldots,K_t)$ are recourse variables with negative coefficients. where u_{st} is expectation and σ_{st} is standard variation of random parameters with normal distributions; $a_{ijt}^{\pm}$, b_{rth}^{+}, $c_{jt}^{\pm}$ and $d_{jtk}^{\pm}$ are real-number coefficients parameters; where ϕ^{-1} is the inverse cumulative distribution function of a standard normal random variable. Solutions of

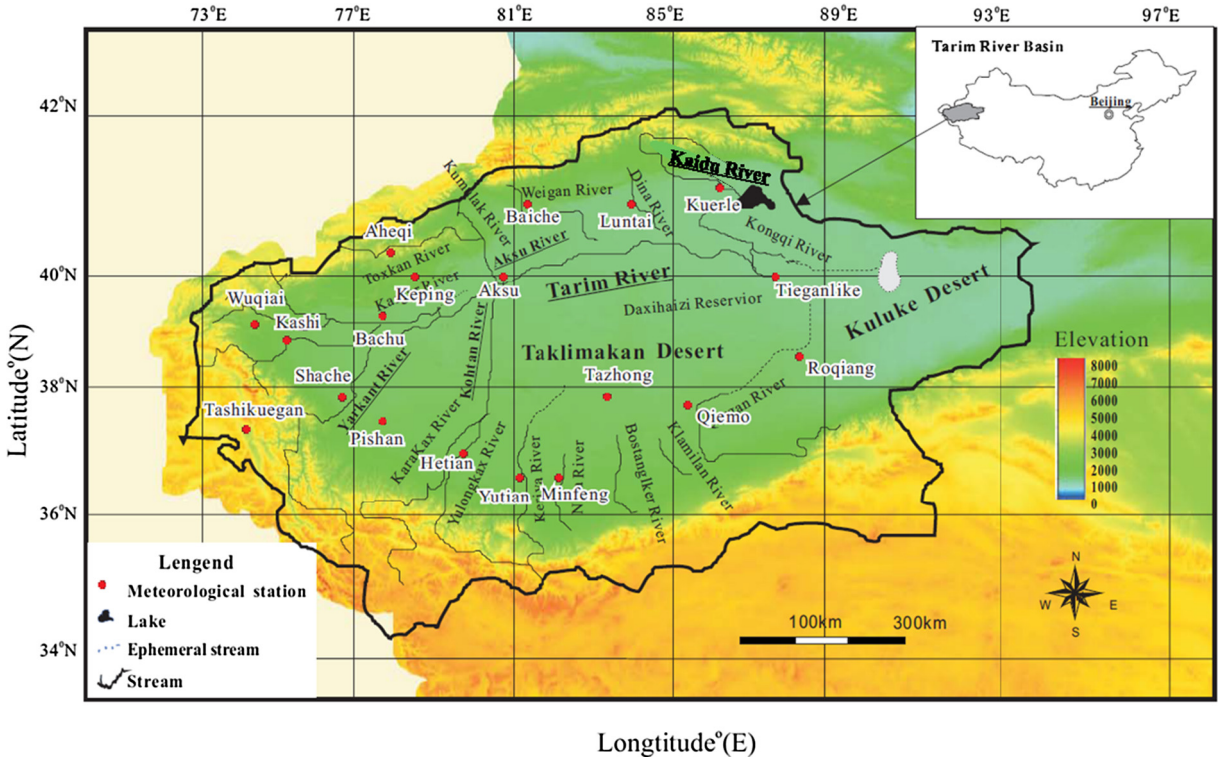

Fig. 2. Study watershed in northwestern China.

Table 1
Different probability levels.

Case	Individual probability				
	q_1 (low level)	q_2 (low-medium level)	q_3 (medium level)	q_4 (medium-high level)	q_5 (high level)
1	0.01	0.01	0.01	0.01	0.01
2	0.02	0.02	0.02	0.02	0.02
3	0.04	0.04	0.04	0.04	0.04
4	0.06	0.06	0.06	0.06	0.06
5	0.08	0.08	0.08	0.08	0.08
6	0.10	0.10	0.10	0.10	0.10
7	0.12	0.12	0.12	0.12	0.12
8	0.14	0.14	0.14	0.14	0.14
9	0.16	0.16	0.16	0.16	0.16
10	0.18	0.18	0.18	0.18	0.18
11	0.20	0.20	0.20	0.20	0.20

Table 2
Economical inputs over the planning period (unit US$/$10^6$ m^3).

Time period	Water allocation target ($W_{it}^{\pm}$)	Maximum allowable allocation ($W_{it\max}^{\pm}$)	Net benefit when water demand is satisfied ($B_{it}^{\pm}$)	Reduction of net benefit when demand is not delivered ($C_{it}^{\pm}$)
t = 1 (2016–2020)	[2923.8, 3378.8]	6000.0	[425.7, 600.6]	[785.7, 831.0]
t = 2 (2021–2025)	[2947.6, 3420.1]	6000.0	[463.4, 638.3]	[816.3, 862.0]
t = 3 (2026–2030)	[2971.4, 3461.4]	6000.0	[501.1, 676.0]	[846.9, 893.0]
t = 4 (2031–2035)	[2995.2, 3502.7]	6000.0	[538.8, 713.7]	[877.4, 924.0]
t = 5 (2036–2040)	[3019.0, 3544.0]	6000.0	[576.5, 751.4]	[908.0, 955.0]
t = 6 (2041–2045)	[3042.8, 3585.3]	6000.0	[614.2, 789.1]	[938.6, 986.0]
t = 7 (2046–2050)	[3066.6, 3626.6]	6000.0	[651.9, 826.8]	[969.6, 1017.0]
t = 8 (2051–2055)	[3090.4, 3667.9]	6000.0	[689.6, 864.5]	[999.7, 1048.0]
t = 9 (2056–2060)	[3114.2, 3709.2]	6000.0	[727.3, 902.2]	[1030.3, 1079.0]
t = 10 (2061–2065)	[3138.0, 3750.5]	6000.0	[765.0, 939.9]	[1060.9, 1110.0]
t = 11 (2066–2070)	[3161.8, 3791.8]	6000.0	[802.7, 977.6]	[1091.5, 1141.0]
Mean value	[3042.8, 3585.3]	6000.0	[614.2, 789.1]	[938.6, 986.0]

$x^{+}_{jt\text{opt}}(j=1,2,\ldots,j_1)$, and $x^{-}_{jt\text{opt}}(j=j_1+1,j_1+2,\ldots,n_1)$, $y^{-}_{jtk\text{opt}}(j=1,2,\ldots,j_2$ and $k=1,2,\ldots,K_t)$, and $y^{+}_{jtk\text{opt}}(j=j_2+1,j_2+2,\ldots,n_2$ and $k=1,2,\ldots,K_t)$ can be obtained through solving sub-model (3). Based on the above solutions, the second sub-model corresponding to f^{-} can be formulated as follows:

$$Maxf^{-}=\sum_{t=1}^{T}\left(\sum_{j=1}^{j_1}c^{-}_{jt}x^{-}_{jt}+\sum_{j=j_1+1}^{n_1}c^{-}_{jt}x^{+}_{jt}\right)-\sum_{t=1}^{T}\sum_{k=1}^{K_t}p_{tk}\left(\sum_{j=1}^{j_2}d^{+}_{jtk}y^{+}_{jtk}+\sum_{j=j_2+1}^{n_2}d^{+}_{jtk}y^{-}_{jtk}\right) \quad (4a)$$

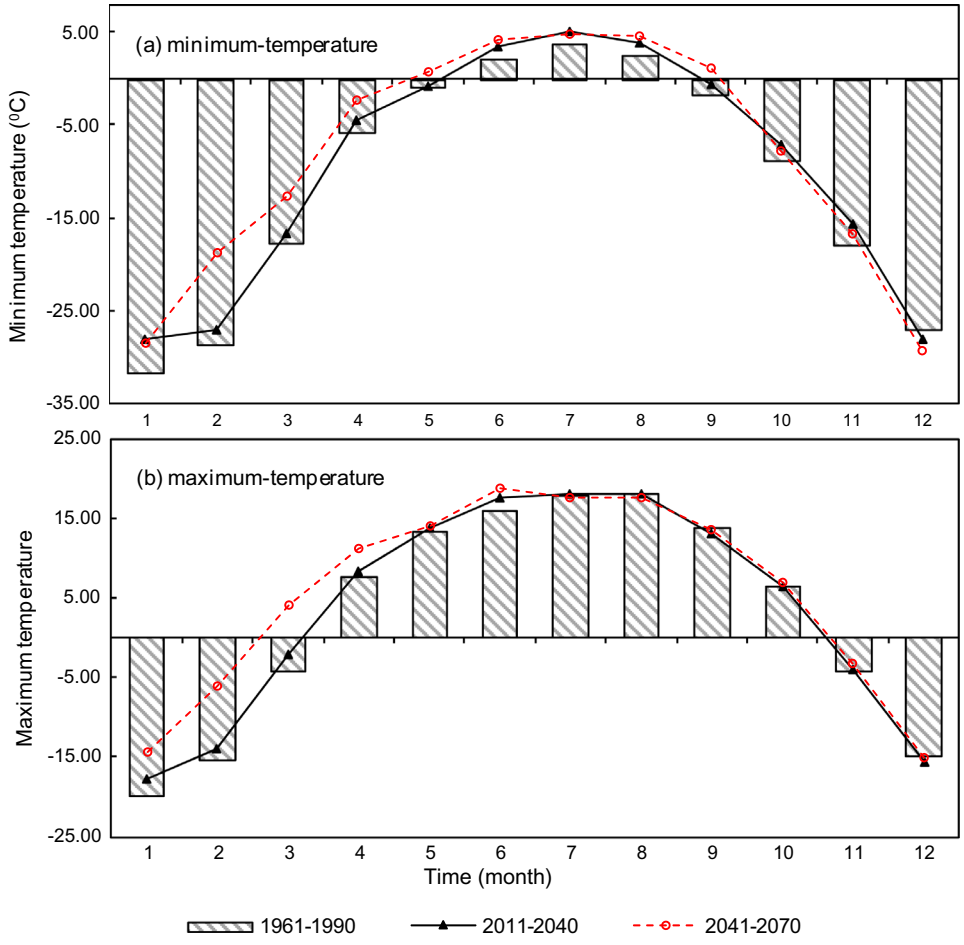

Fig. 3. Downscaled minimum-temperature and maximum-temperature during baseline and future periods.

Table 3
Projected maximum-temperature during baseline and future periods.

	Projected maximum-temperature (°C)								
Station	Baluntay			Bayinbulak			Yanqi		
Period	Baseline (1961–1990)	Future (2016–2040)	Future (2041–2070)	Baseline (1961–1990)	Future (2016–2040)	Future (2041–2070)	Baseline (1961–1990)	Future (2016–2040)	Future (2041–2070)
January	−1.22	−0.46	0.92	−19.83	−17.73	−14.33	−3.50	0.27	1.75
February	1.79	2.82	5.76	−15.47	−13.85	−6.06	2.55	4.57	7.26
March	8.77	10.12	13.36	−4.30	−2.04	4.10	12.21	13.37	16.91
April	16.00	17.01	19.34	7.47	8.28	11.29	20.36	21.49	24.11
May	21.66	21.63	23.46	13.16	13.72	13.92	26.08	26.59	27.74
June	24.85	25.83	26.04	15.89	17.65	18.82	29.20	29.74	30.04
July	26.48	26.53	26.51	17.88	17.99	17.61	30.18	31.26	31.30
August	25.88	26.50	26.66	17.96	18.00	17.47	29.73	30.28	31.20
September	21.08	22.52	25.83	13.63	13.09	13.49	24.92	25.66	28.02
October	14.64	14.81	14.73	6.34	6.43	7.03	17.56	17.98	18.33
November	6.55	7.34	7.60	−4.23	−3.97	−3.17	7.15	9.04	10.43
December	−0.02	0.72	2.47	−15.05	−15.68	−15.22	−1.76	1.12	3.02
Mean	13.87	14.61	16.06	2.79	3.49	5.41	16.22	17.61	19.17

subject to:

$$\sum_{j=1}^{j_1}|a_{rjt}|^{+}\mathrm{Sign}(a_{rjt}^{+})x_{jt}^{-}+\sum_{j=j_1+1}^{n_1}|a_{rjt}|^{-}\mathrm{Sign}(a_{rjt}^{-})x_{jt}^{+}\leqslant b_{rth}^{-}\quad\forall r,\ t,h \tag{4b}$$

$$\sum_{j=1}^{j_1}|a_{ijt}|^{+}\mathrm{Sign}(a_{ijt}^{+})x_{jt}^{-}+\sum_{j=j_1+1}^{n_1}|a_{ijt}|^{-}\mathrm{Sign}(a_{ijt}^{-})x_{jt}^{+}\sum_{j=1}^{j_2}|a'_{ijtk}|^{-}\mathrm{Sign}(a'^{-}_{ijtk})y_{jtk}^{+}\sum_{j=j_2+1}^{n_2}|a'_{ijtk}|^{+}\mathrm{Sign}(a'^{+}_{ijtk})y_{jtk}^{-}\leqslant\tilde{w}_{itk}^{-}\quad\forall i,t;\ k=1,2,\ldots,K_t \tag{4c}$$

$$\left[\sum_{j=1}^{j_1}|a_{sjt}|^{+}\mathrm{Sign}(a_{sjt}^{+})x_{jt}^{-}+\sum_{j=j_1+1}^{n_1}|a_{sjt}|^{-}\mathrm{Sign}(a_{sjt}^{-})x_{jt}^{+}\right](u_{st}+\sigma_{st}\phi^{-1}(1-q_s))\leqslant b_{sth}^{-}\quad\forall s,t,h \tag{4d}$$

$$0\leqslant x_{jt}^{-}\leqslant x_{jt\mathrm{opt}}^{+}\quad\forall t;\ j=1,2,\ldots,j_1 \tag{4e}$$

$$x_{jt}^{+}\geqslant x_{jt\mathrm{opt}}^{-}\quad\forall t;\ j=j_1+1,j_1+2,\ldots,n_1 \tag{4f}$$

$$y_{jtk}^{+}\geqslant y_{jtk\mathrm{opt}}^{-}\quad\forall t;\ j=1,2,\ldots,j_2;\ k=1,2,\ldots,K_t \tag{4g}$$

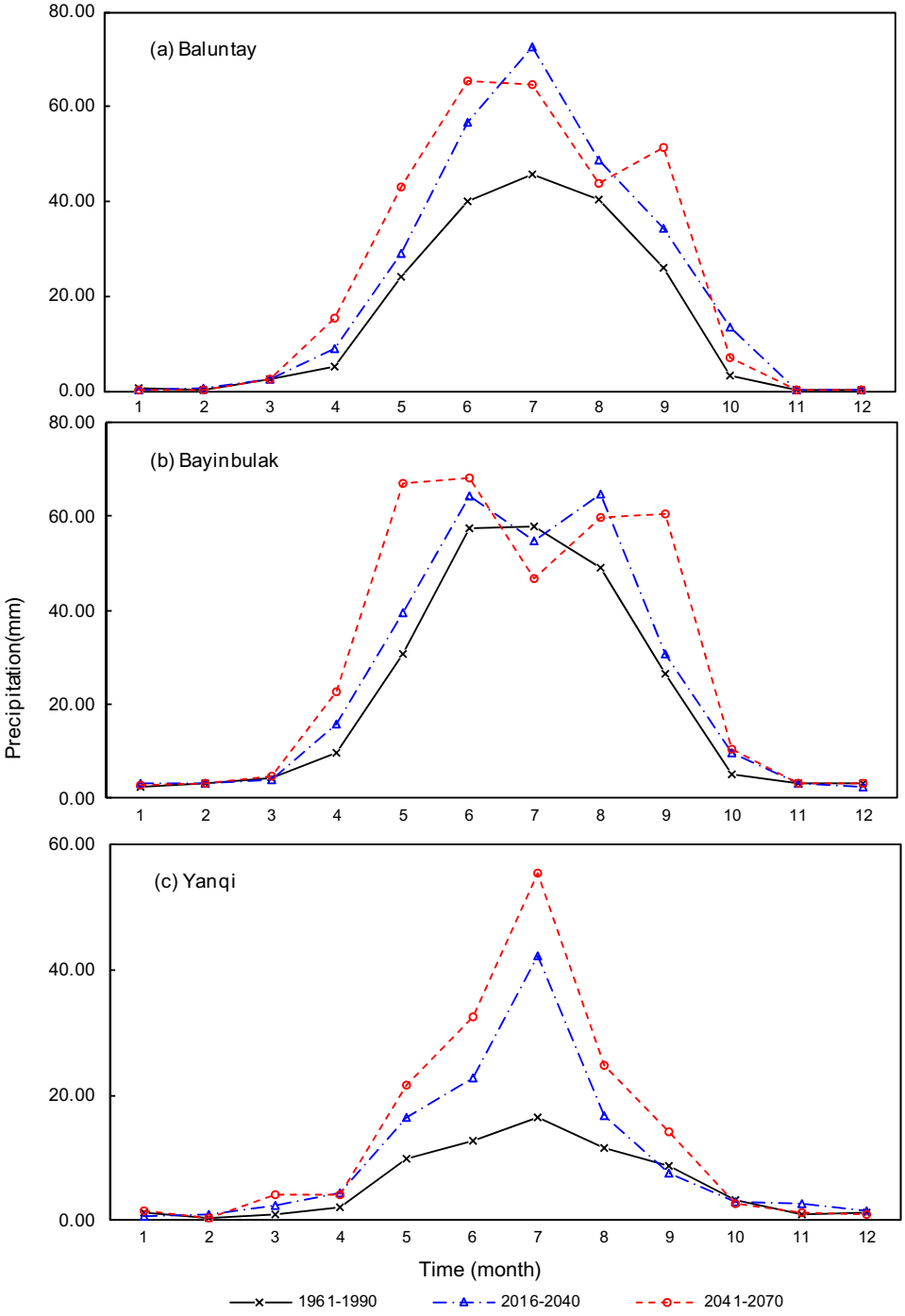

Fig. 4. Downscaled precipitation at the Baluntay, Bayinbulak and Yanqi stations during baseline and future periods.

$$0 \leqslant y^{-}_{jtk} \leqslant y^{+}_{jtkopt} \quad \forall t;\ j = j_2+1, j_2+2, \ldots, n_2;\ k = 1,2,\ldots,K_t \tag{4h}$$

Solutions of $x^{-}_{jtopt}(j = 1,2,\ldots,j_1)$, $x^{+}_{jtopt}(j = j_1+1, j_1+2, \ldots, n_1)$, $y^{+}_{jtkopt}(j = 1,2,\ldots j_2$ and $k = 1,2,\ldots,K_t)$, and $y^{-}_{jtkopt}(j = j_2+1, j_2+2,\ldots,n_2$ and $k = 1,2,\ldots,K_t)$ can be obtained through solving sub-model (4). Therefore, combining solutions of sub-models (3) and (4), solution for the IMC model can be expressed as follows:

$$x^{\pm}_{jtopt} = [x^{-}_{jtopt}, x^{+}_{jtopt}] \quad j = 1,2,\ldots,n_1;\ \forall t \tag{5a}$$

$$y^{\pm}_{jtkopt} = [y^{-}_{jtkopt}, y^{+}_{jtkopt}] \quad j = 1,2,\ldots,n_2;\ k = 1,2,\ldots,K_t;\ \forall t \tag{5b}$$

$$f^{\pm}_{opt} = [f^{-}_{opt}, f^{+}_{opt}] \tag{5c}$$

3. Case study

The Kaidu River originates from the south of the Tian Shan Mountain and is one of the four mainstreams of the longest inland river (the Tarim River), in China. The Kaidu watershed, enclosed between 42°14′–43°21′ N latitudes and 82°58′–86°05′ E longitudes, is located in the Xinjiang Uyghur Autonomous Region of northwest China and is near the Taklimakan Desert. Kaidu watershed drains an area of about 19×10^3 km^2, with an average elevation of 3100 m (Fig. 2). The climate of Kaidu watershed is characterized mainly by dryness and coldness. Its annual average precipitation is less than 500 mm and pan evaporation is >1100 mm, where evaporation exceeds precipitation leading to a dry desert climate (Ling et al., 2013). Under the general background of global warming, the climate in Kaidu watershed has been undergoing significant changes, such as increased temperature and precipitation, added river runoff volumes, accelerated retreat of glaciers, and increased lake water surface elevation and area. The increasing trend of air temperature over the past 50 years in the Kaidu watershed has been indicated, with a jump around 1986 (Deng et al., 2015).

As the unique high alpine cold climate and topography, the streamflow of Kaidu watershed is principally provided by high mountain precipitation and seasonal snow and glacier melting; the climate factors directly affecting the recharge of the river are temperature and precipitation. Assessments of variation and vulnerability of runoff are essential for future planning because changes in climatic processes affect both water availability and water demand. Recent studies identified the Kaidu watershed as one of the world's water crisis hot-spots. It is an inland area that water crisis is aggravated due to climatic change, population growth, agricultural exploration, and economic development. It is desirable for projection of future range of climate change scenarios in order to evaluate the vulnerability of water resources system and the effectiveness of different adaptation strategies in managing climate-related stresses.

Besides, uncertainties exist in water resources systems, such as hydrological processes, water conservancy facilities, water con-

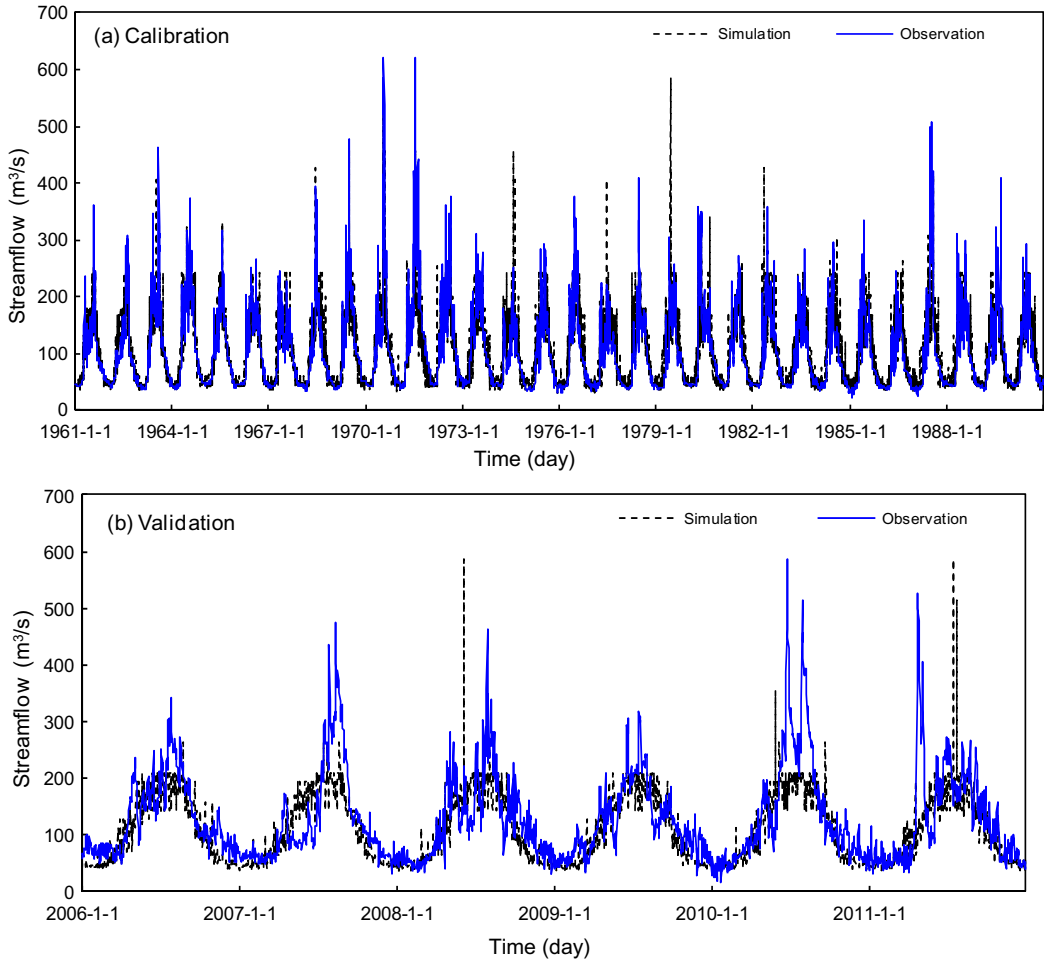

Fig. 5. Comparison of simulated and observed streamflows during (a) calibration, and (b) validation periods.

sumption and water supply, and socioeconomic activities. In the study system, the streamflow is random variable with known probability distributions; the relevant water allocation plan would be of dynamic feature over a multi-period context; and uncertainties also provide as intervals for water-allocation targets and economic data. Therefore, the developed ISO is an effective tool for forecasting or allocating water resources under climate change, which can support water allocation more efficiently to relieve the pressure of water conflicts in such an arid region. A number of cases associated with different probabilities (listed in Table 1) are examined. Correspondingly, the probability (q, $q \in [0,1]$) is a prescribed level of probability for each constraint imposing a condition that the constraint is satisfied with at least a probability of $1 - q$. Table 2 shows the economic inputs during different periods. The time horizon of this study is divided into eleven planning periods (with each five years).

4. Result and discussion

4.1. Downscaled climate scenarios

The developed ISO approach was employed for transferring atmospheric simulation outputs to acquire high-resolution climate

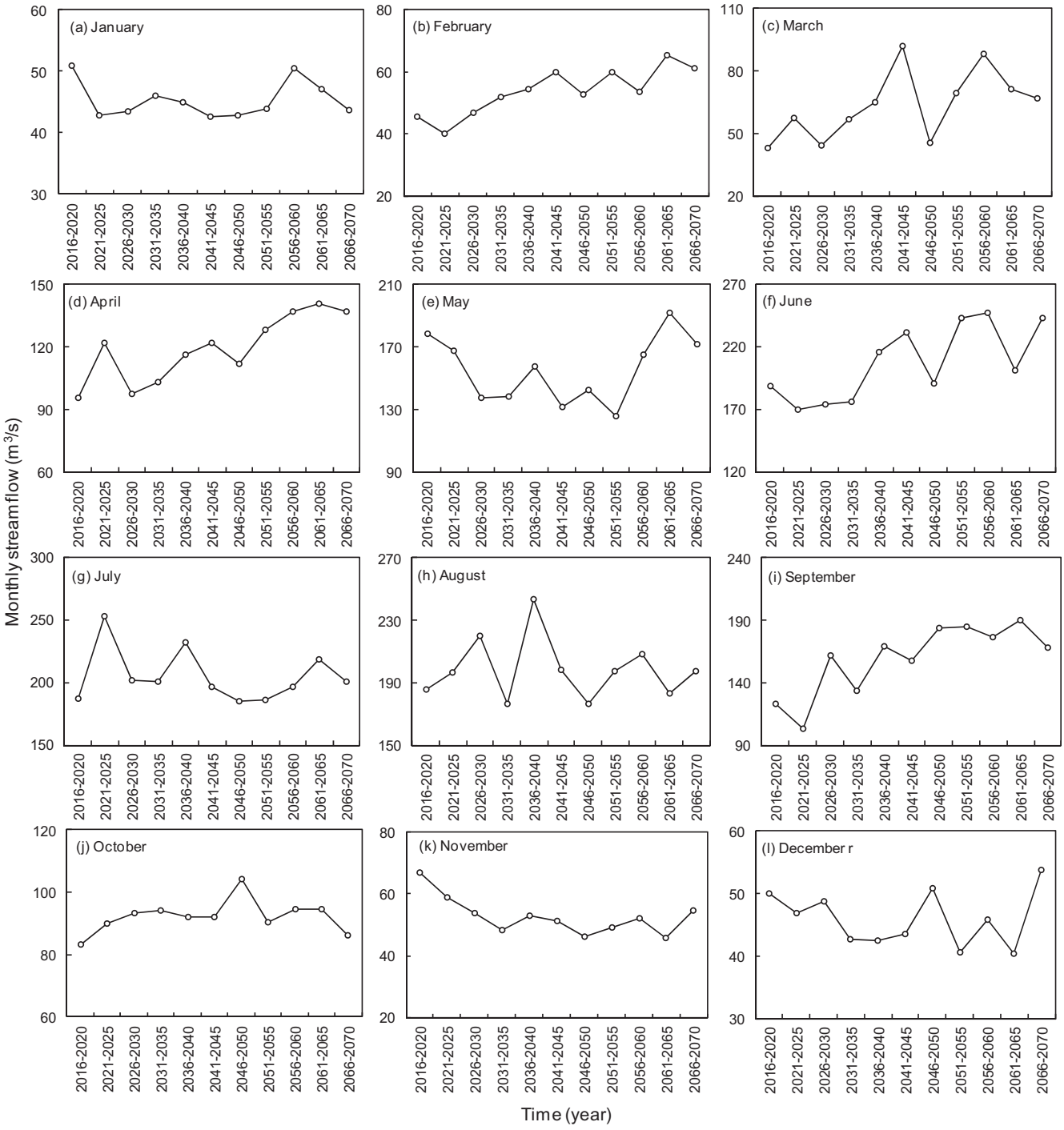

Fig. 6. Comparison of simulated streamflows during prediction period (2016–2070).

projections during baseline (1961–1990) and future (2016–2070) periods at the Kaidu watershed. Fig. 3 shows the simulated results of monthly minimum and maximum temperatures during baseline and future periods. Results indicate that minimum and maximum temperatures would both increase from baseline to future (as shown in Table 3). For example, the minimum temperature values of August in future would be 3.87 (2016–2040) and 4.61 °C (2041–2070), which are larger than that (i.e., 2.64 °C) during the baseline (1961–1990) (Fig. 3). Generally, meteorological projections enable to reflect wet, dry, warm, or cool conditions, and facilitate simulation/prediction of future climate change in the Kaidu watershed.

Fig. 4 presents monthly precipitation for different stations (Baluntay, Bayinbulak and Yanqi) during baseline (1961–1990) and future (2016–2070) periods. Results discover that precipitation would increase. For instance, the precipitation values for June would be 40.19 mm (1961–1990), 56.60 mm (2016–2040) and 65.52 mm (2041–2070) for Baluntay. Additionally, the monthly mean values would be 14.22 mm (1961–1990), 19.03 mm (2016–2040) and 22.51 mm (2041–2070), implying an increase of perturbed climatic time-series for future. Besides, results indicate that projected climate change scenarios are variable for different stations. For example, the projected precipitation for December would be 0.2 mm (Baluntay), 3.0 mm (Bayinbulak), and 1.1 mm (Yanqi). The spatial heterogeneity of precipitation distribution is attributed to the complexity of topography and variation in elevations.

4.2. Future water resources conditions

In this study, through using datasets of meteorological factors (minimum and maximum temperatures, and precipitation) as inputs, the daily climate-streamflow hydrological simulation were calibrated and validated. Correspondingly, trends of daily streamflows in calibration (1961–1990), validation (2006–2011) and future (2016–2070) periods would be simulated in the Kaidu watershed. Fig. 5 shows the daily observed and simulated streamflows during calibration and validation periods. The *NSE* values would be 0.68 (calibration), and 0.65 (validation); which indicating the good agreement between observed and simulated streamflows. The coefficient of correlation (R^2) for calibration and validation would be 1.68% and 4.11%, respectively; with a satisfactory fitting for streamflow simulation. Fig. 6 presents comparison of simulated streamflows during prediction period (2016–2070). Table 4 lists the occurrence probability of streamflow (p_{tk}), over the planning period (2016–2070). Table 5 shows the simulated streamflows, i.e., random water availability with probability p_{tk}, in the future periods.

In this study, totally 110 scenarios for water resources management were investigated. It can be disclosed that water deficit exists in future for the study watershed. Fig. 7 presents the allocated water resources under different cases 1–11, when streamflows are at low and low-medium levels. Fig. 8 shows the allocated water resources at medium, medium-high and high levels under cases 1–11. Results indicate that allocated water resources would be changed under different cases. For instance, the allocated water at low level during 2016–2020 would be [1574.6, 2549.7] (case 1), [1594.0, 2572.1] (case 2), [1615.6, 2597.1] (case 3), [1629.0, 2612.6] (case 4), [1638.6, 2623.8] (case 5), [1646.4, 2632.7] (case 6), [1653.3, 2640.7] (case 7), [1659.2, 2647.5] (case 8), [1665.1, 2654.4] (case 9), [1669.1, 2659.0] (case 10), and [1674.1, 2664.7] (case 11) $\times 10^6$ m^3 (Fig. 8).

It can be found that the lowest amount of allocated water would be under case 1, while the highest one would be under case 11. For example, under case 1, the allocated water during 2066–2070 would be [1879.8, 2868.3] (low), [2236.8, 3124.2] (low-medium),

Table 4
The occurrence probability of streamflow over the planning period.

Time period	Flow level				
	Low (L)	Low-medium (L-M)	Medium (M)	Medium-high (M-H)	High (H)
t = 1 (2016–2020)	0.173	0.198	0.269	0.195	0.165
t = 2 (2021–2025)	0.168	0.211	0.259	0.205	0.157
t = 3 (2026–2030)	0.167	0.195	0.253	0.217	0.168
t = 4 (2031–2035)	0.164	0.215	0.250	0.218	0.153
t = 5 (2036–2040)	0.169	0.192	0.244	0.216	0.179
t = 6 (2041–2045)	0.153	0.186	0.267	0.211	0.183
t = 7 (2046–2050)	0.183	0.188	0.231	0.218	0.180
t = 8 (2051–2055)	0.167	0.176	0.267	0.217	0.173
t = 9 (2056–2060)	0.163	0.183	0.258	0.218	0.178
t = 10 (2061–2065)	0.167	0.184	0.265	0.215	0.169
t = 11 (2066–2070)	0.163	0.193	0.263	0.216	0.165
Mean value	0.167	0.193	0.257	0.213	0.170

Table 5
Streamflows over the planning period (unit 10^6 m^3).

Time period	Flow level				
	Low (L)	Low-medium (L-M)	Medium (M)	Medium-high (M-H)	High (H)
t = 1 (2016–2020)	[2657.2, 3071.1]	[3071.1, 3377.8]	[3377.8, 3792.6]	[3792.6, 4163.5]	[4163.5, 4571.8]
t = 2 (2021–2025)	[2917.2, 3297.8]	[3297.8, 3579.6]	[3579.6, 3928.6]	[3928.6, 4234.7]	[4234.7, 4577.7]
t = 3 (2026–2030)	[2620.1, 3061.3]	[3061.3, 3408.4]	[3408.4, 3817.5]	[3817.5, 4177.0]	[4177.0, 4583.9]
t = 4 (2031–2035)	[2668.3, 3029.2]	[3029.2, 3294.0]	[3294.0, 3615.2]	[3615.2, 3886.2]	[3886.2, 4228.1]
t = 5 (2036–2040)	[2974.8, 3487.5]	[3487.5, 3814.5]	[3814.5, 4199.9]	[4199.9, 4551.5]	[4551.5, 4987.9]
t = 6 (2041–2045)	[2803.0, 3207.9]	[3207.9, 3522.7]	[3522.7, 3874.2]	[3874.2, 4159.6]	[4159.6, 4519.0]
t = 7 (2046–2050)	[2922.0, 3308.8]	[3308.8, 3612.3]	[3612.3, 3938.2]	[3938.2, 4253.6]	[4253.6, 4594.2]
t = 8 (2051–2055)	[3037.8, 3385.8]	[3385.8, 3654.6]	[3654.6, 3973.0]	[3973.0, 4257.5]	[4257.5, 4576.4]
t = 9 (2056–2060)	[3191.1, 3602.8]	[3602.8, 3881.2]	[3881.2, 4240.8]	[4240.8, 4554.4]	[4554.4, 4913.5]
t = 10 (2061–2065)	[3252.7, 3561.8]	[3561.8, 3792.0]	[3792.0, 4054.1]	[4054.1, 4286.9]	[4286.9, 4581.8]
t = 11 (2066–2070)	[3024.9, 3454.9]	[3454.9, 3763.1]	[3763.1, 4148.8]	[4148.8, 4457.9]	[4457.9, 4850.4]
Mean value	[2915.4, 3315.3]	[3315.4, 3609.1]	[3609.1, 3962.1]	[3962.1, 4271.2]	[4271.2, 4635.0]

[2492.7, 3444.4] (medium), [2812.9, 3701.0] (medium-high), and [3069.5, 3791.8] (high) $\times 10^6$ m^3. In contrast, the allocated water under case 11 would be [1993.1, 2997.7] (low), [2366.2, 3265.2] (low-medium), [2633.7, 3599.8] (medium), [2968.3, 3791.8] (medium-high), and [3236.5, 3791.8] (high) $\times 10^6$ m^3; which indicating an increase trend. Furthermore, the allocated water resources in different periods are variable. Therefore, vulnerability assessments of water resources can help evaluate the susceptibility of water systems to potential climate change threats and identify effective adaptation strategies to reduce or mitigate the risk of serious consequences from adverse climate impacts.

Figs. 9 and 10 show the water shortage amount under cases 1 and 2 (q = 0.01 and q = 0.02), cases 10 and 11 (q = 0.18, and q = 0.20), when streamflows are at low, low-medium, medium, medium-high and high levels. For instance, the water shortage amount under case 1 at low level would vary from [682.2, 1629.7] to [923.5, 1912.0] $\times 10^6$ m^3 in 2016–2070; which indicating insufficient available water resources result in water deficiency. In contrast, when the streamflow is at high level, the water shortage amount under low level would vary from [0, 535.9] to [0, 822.9] $\times 10^6$ m^3. Results show that water deficit would occur, although available water is high.

Besides, the water deficit would occur over the planning period. As shown in Figs. 9 and 10, water shortage amount under case 2 at low level would be [897.5, 1898.5] (2026–2030), [717.8, 1651.5] (2031–2035), [623.1, 1684.0] (2036–2040), [898.6, 1869.2] (2041–2045), [855.4, 1810.9] (2046–2050), [832.2, 1755.2] (2051–2055), [691.8, 1668.1] (2056–2060), [767.4, 1657.8] (2061–2065), and [898.2, 1889.9] (2066–2070) $\times 10^6$ m^3. There are no obvious changes of future water deficit under climate change impacts. In other words, with population increase and economic expansion, water shortage would become evident during future. Consequently, the exposure of water resources to drought would increase, because variability of available water. It can be explained that the large-scale development and utilization of water resources would aggravate water deficit, causing a series of ecological environment problems (Li et al., 2016).

Result can also be found that with the highest risk of violating the water target demands (i.e., q = 0.20), the water-shortage patterns under cases 9, 10 and 11 are different from it under cases 1 and 2. For instance, the water shortage amounts at low level during period 2 (t = 2, 2021–2025) would be [682.2, 1629.7] (case 1, q = 0.01), [658.1, 1608.4] (case 2, q = 0.02), [569.8, 1530.3] (case 9, q = 0.16), [564.9, 1525.9] (case 10, q = 0.18), and [558.7, 1520.4] (case 11, q = 0.20) $\times 10^6$ m^3. Results disclose that water shortage amount would be lowest under case 11, while it would be highest under case 1. Moreover, it is indicated that the effects of individual probability levels on the water resources results would vary in different cases. It can be explained that a higher level of individual probability corresponds to a relaxed decision domain, a more reliability of sufficient water supply, which results in a higher satisfactory degree of water demands constraint and lower risk of water-shortage.

It can be discovered that different characteristics of water shortage exist in different levels. When the sreamflow is at low level, the water shortage amount would be larger. For instance, water shortage under case 1 at low level would be [682.2,

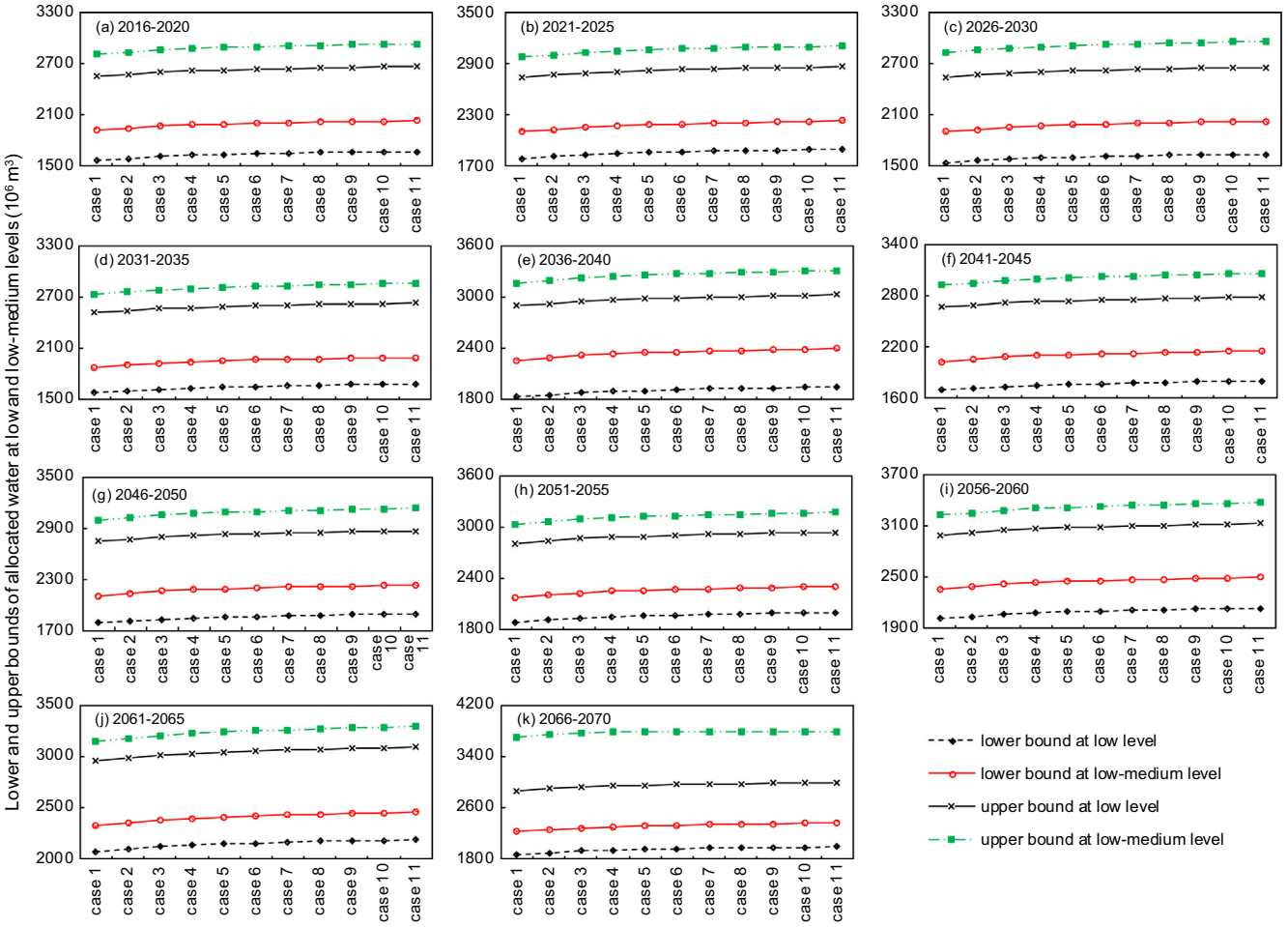

Fig. 7. Allocated water resources (10^6 m^3) at low and low-medium levels under different cases.

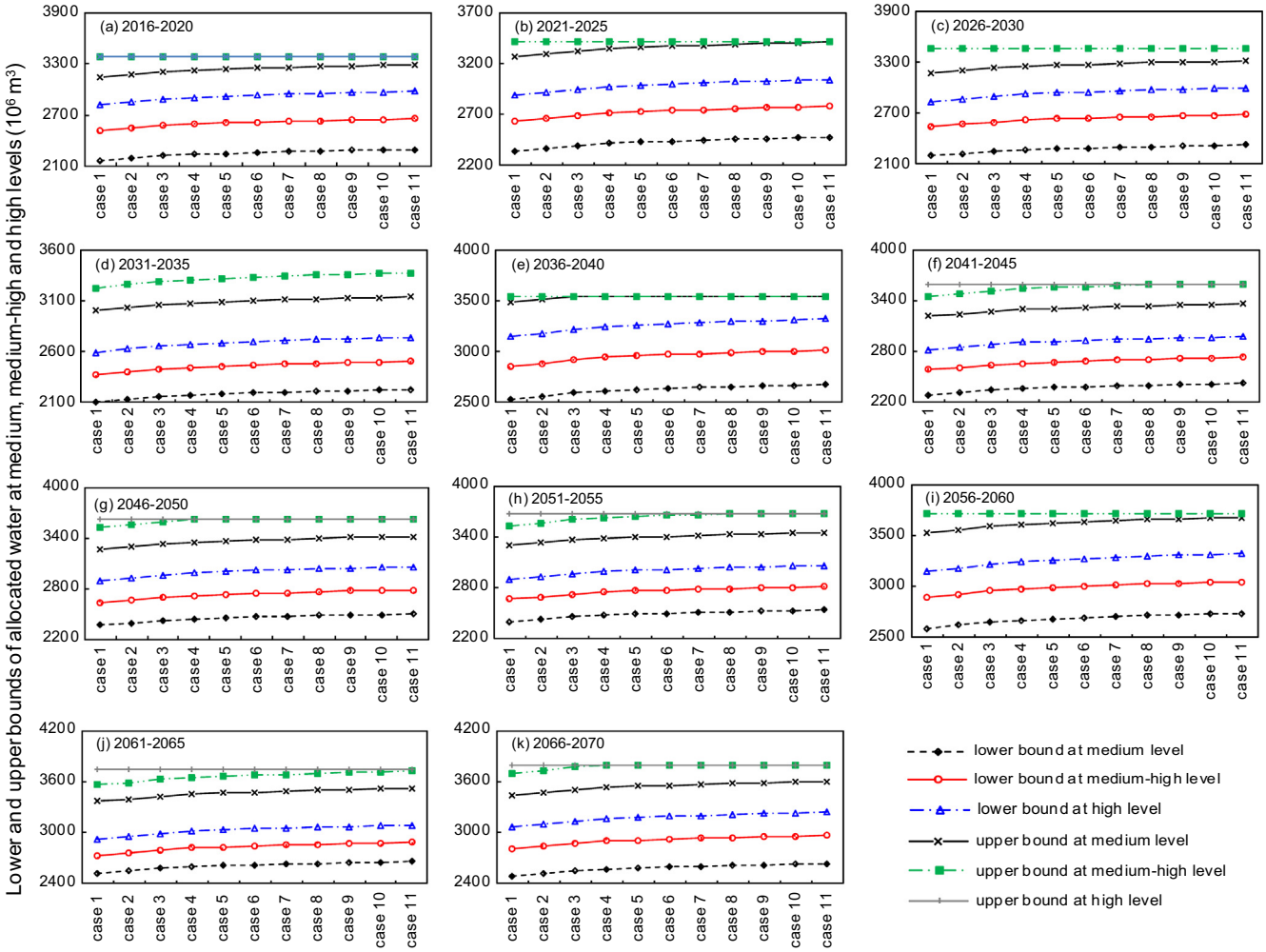

Fig. 8. Allocated water resources (10^6 m^3) at medium, medium-high and high levels under different cases.

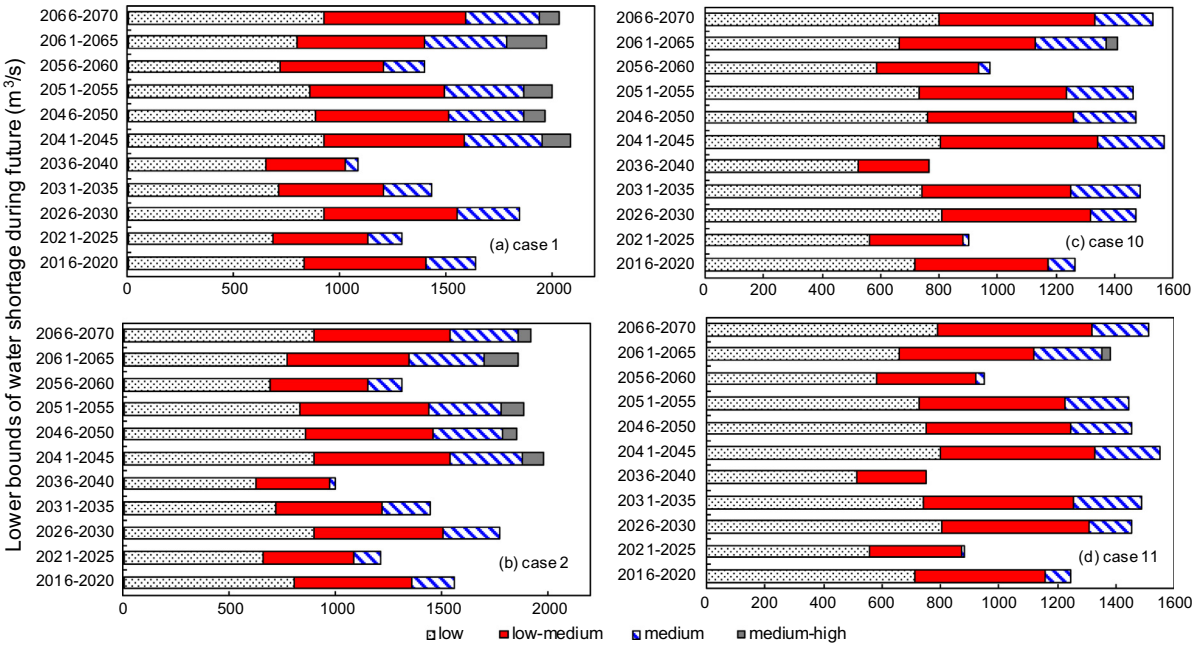

Fig. 9. Lower bounds of water shortage amount (10^6 m^3) under (a) case 1, (b) case 2, (c) case 10 and (d) case 11 at different levels.

1629.7] (t = 2, 2021–2025) × 10^6 m^3. In contrast, the water shortage amounts would be [448.2, 1313.7] (low-medium), [158.5, 1079.7] (medium), [0.0, 790.0] (medium-high), and [0.0, 535.9] (high) × 10^6 m^3; which indicating a decreasing trend. Generally, results can be found that the more the inflow amount decreases, the higher the estimated water shortage rates are.

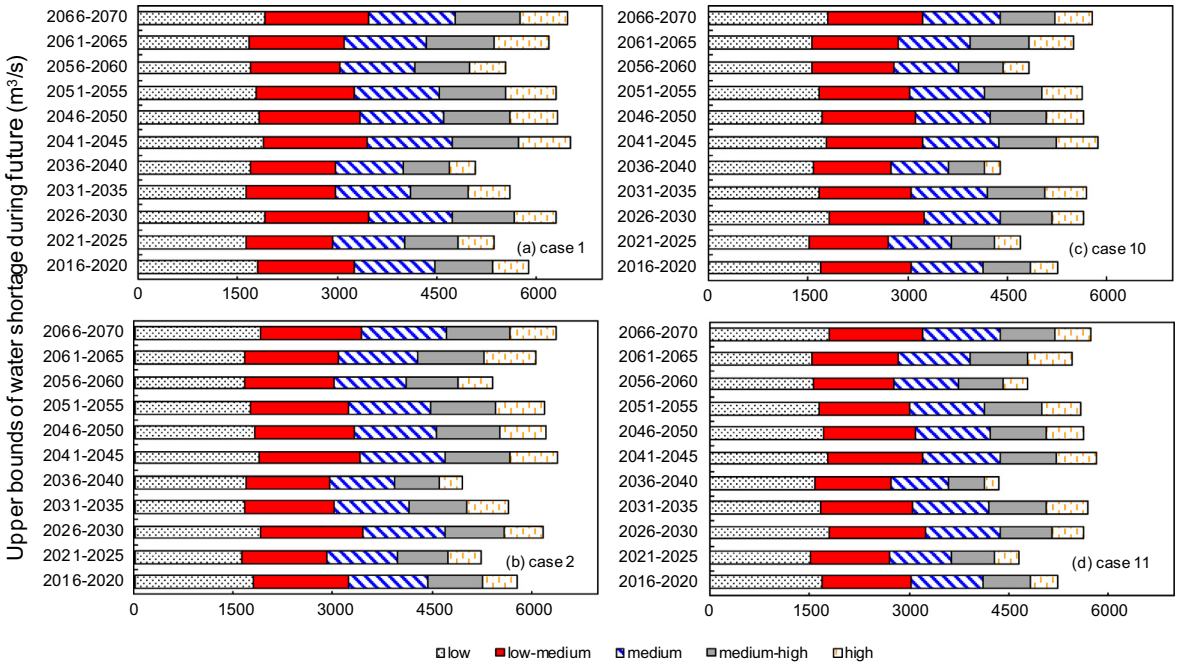

Fig. 10. Upper bounds of water shortage amount (10^6 m^3) under (a) case 1, (b) case 2, (c) case 10 and (d) case 11 at different levels.

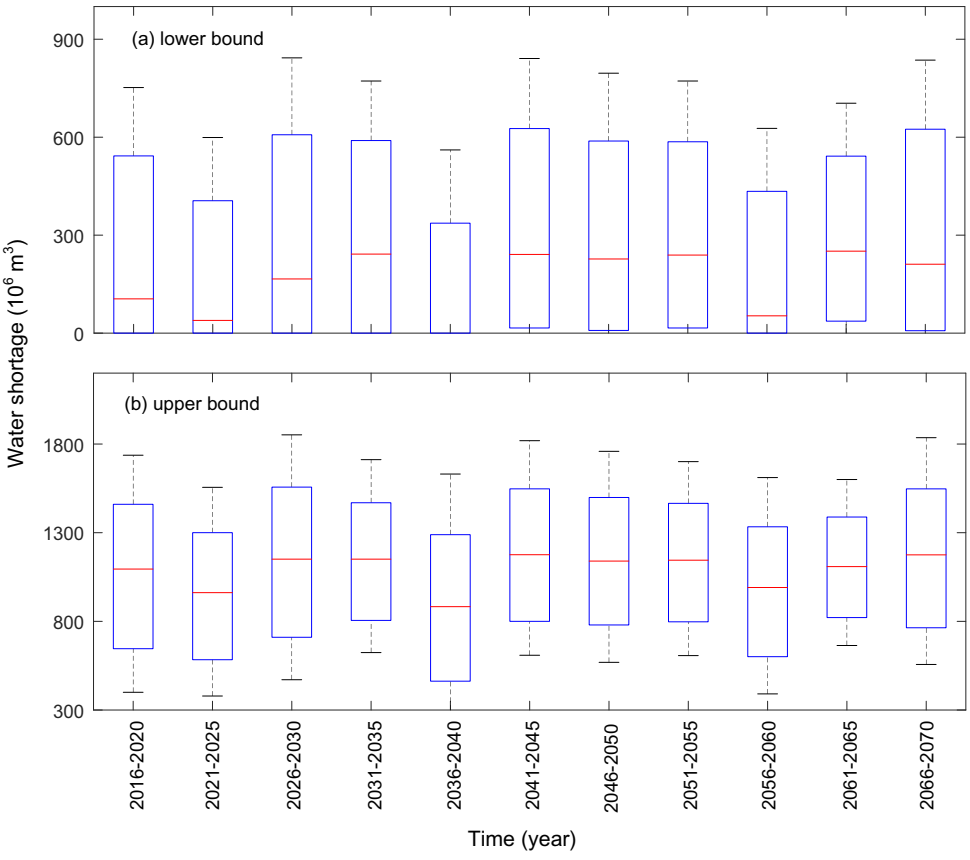

Fig. 11. The boxplots of changes in water shortage.

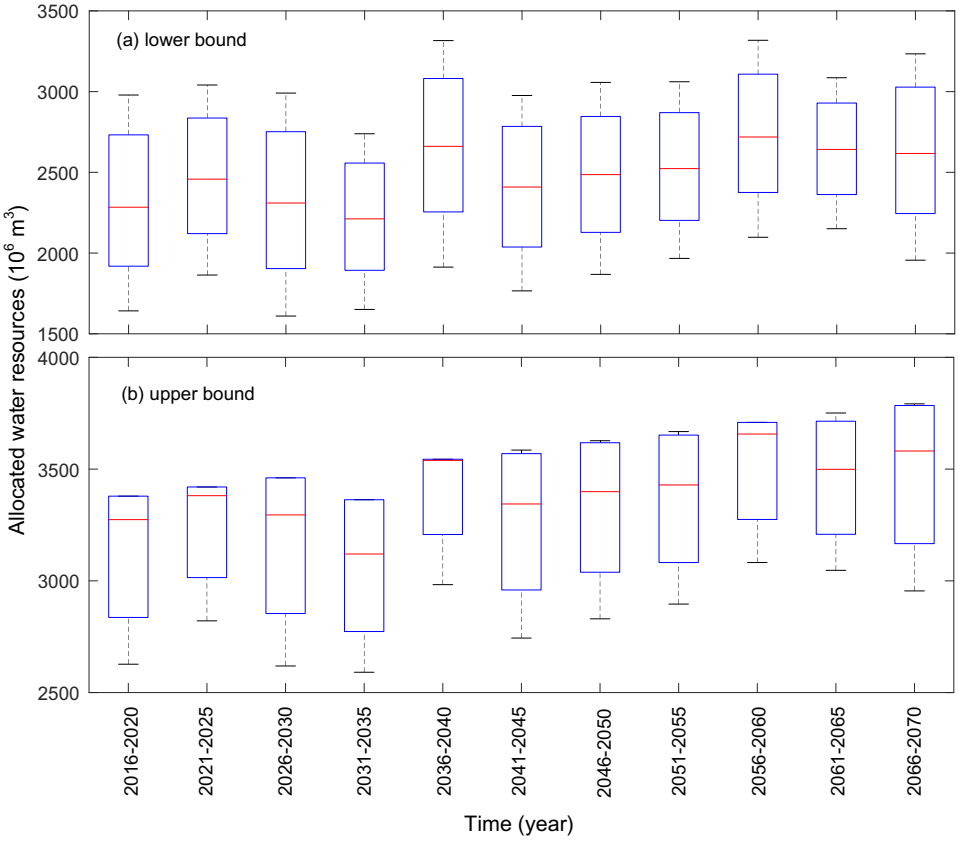

Fig. 12. The boxplots of changes in allocated water resources.

4.3. Uncertainties of water deficit

Fig. 11 shows results of water deficit during 2016–2070 in the study watershed. Mean values and variability ranges of water deficit under different streamflows are varied over the planning periods. Correspondingly, dynamics of water shortage can be reflected, and should be taken into consideration in water resources management. In fact, as the increase in precipitation falls short of temperature increase, evaporation may intensify and thus aggravate drought (Xu et al., 2004). Additionally, variability of water demand is one main factor contributing the risk of water shortage. The water demand gets its maximum value due to that the high temperature resulting in the high amount of evaporation and transpiration; moreover, the most sensitive growth period of plants to water deficit is in the dry season (April, May and June) (Karamouz et al., 2012).

Fig. 12 presents water-resources allocation pattern. Results discover that increasing trends of allocated water resources under climate change impacts exist during different future periods. For instance, the allocated water would be highest during 2066–2070; while the lowest amount would be during 2016–2020. The possible reason for the different performances of water resources variability over the planning period is that changes of meteorological variables (minimum and maximum temperatures and precipitation) pose significant impacts on future available water, thus leading to changes of allocated water. It can be analyzed from three aspects: (i) precipitation runoff occurs heavily and snowmelt water reduces significantly during the summer and autumn seasons, thereby reducing the proportion of snowmelt runoff; (ii) increasing air temperatures have resulted in a decrease in the proportion of solid precipitation and enhanced snowmelt; and (iii) temperature increases during spring season have a relative more positive effect on streamflow than the other seasons because streamflow is primarily supplied by the snowmelt water.

5. Conclusions

In this study, an integrated simulation-optimization (ISO) method has been developed for assessing climate change impacts on water resources allocation. The developed ISO incorporates the meteorological projection from multi-ensemble GCMs, a daily climate-streamflow hydrological simulation, and an interval-multistage chance-constrained (IMC) optimization within a general framework. The advantages of ISO are as follows: (1) it can help investigate the uncertainty in projected climate changes, through extracting the atmospheric simulation outputs from multi-ensemble of GCMs and, then, to transfer large-scale climate variables to create watershed-scale meteorological projections; (2) through employing the daily climate-streamflow hydrological simulation, it can reflect the nonlinear relationship between hydrological variable (e.g., streamflow) and meteorological factors (e.g., precipitation and temperature) in hydrological processes; and (3) it can reflect uncertainties in water management scenarios and system-violation risks, through employing techniques of multi-stage stochastic programming and individual probabilistic constraints.

Based on the proposed ISO approach, a case study for evaluating the climate change impacts on water resources in the Kaidu watershed (located in northwest China) has been conducted. Precipitation and temperature variations during baseline (1961–1990), recent (2006–2011), and future (2016–2070) periods with respect to climate change effects are assessed using watershed-scale simulation results, which are transferred from the multi-ensemble of

GCMs (CCSM, HadCM3 and MRI-CGCM). Correspondingly, the ISO is able to simulate and capture monthly patterns of hydrometeorological variables (minimum temperature, maximum temperature and precipitation). Using datasets of meteorological factors (minimum and maximum temperatures, and precipitation) as inputs, the daily climate-streamflow hydrological simulation/prediction can be employed for streamflow simulating during calibration (1960–1990), validation (2006–2011) and prediction (2016–2070). It can be found that increase trends of temperature and precipitation exist during future period (2016–2070). Besides, available amounts of water resources would increase as precipitation increases and higher temperature. For instance, the increase in precipitation would reduce the drought conditions and increase the amount of available water.

The developed ISO has been employed for water-resources management, through utilizing individual probabilities to present risk of violating the water target demands and various policy scenarios within a multistage context. Since different individual probabilities associated with different admissible risks of violating the uncertain available water constraints; consequently, results indicate that various water allocation and water shortage patterns under 110 scenarios exist in future period (2016–2070). For example, with the highest risk of violating the water target demands (i.e., case 11, $q = 0.20$), the water shortage pattern during 2016–2020 would be $[923.5, 1912.0] \times 10^6\ m^3$, lower than $[829.1, 1804.2] \times 10^6\ m^3$ when the constraint-violation risk is 0.01 (i.e., case 1). Besides, results discover that from the 2016 to 2070, the drought conditions would be vulnerable, with large amount of water shortage. Correspondingly, water deficit in such an arid region would occur under changing climate, which desiring effective water management measures during decision-making processes. Generally, adaptability assessment of water resources under climate change is crucial to identify effective adaptive measures for integrated management of water resources.

Acknowledgements

This research was supported by the Natural Science Foundation of China (51779008), and the National Key R&D Program of China (2016YFA0601500 and 2016YFC0502800), and the Interdiscipline Research Founds of Beijing Normal University. The authors are grateful to the editors and the anonymous reviewers for their insightful comments and suggestions.

Appendix A.

In SCA, sample sets of predictors are cut or merged into new sets, and values of predictands are used as references to judge into which new set a sample in the parent set will enter. In detail, the clustering criterion is the *F* test based on Wilks' likelihood ratio criterion. Let cluster c, which contains n_c samples, be cut into two sub-clusters a and b (a and b contain n_a and n_b samples, respectively, i.e. $n_a + n_b = n_c$). According to Wilks' likelihood-ratio criterion, if the cutting point is optimal, the value of Wilks' Λ ($\Lambda = |U|/|U+V|$) should be the minimum (Kennedy and Gentle, 1981); where U and V are the total-sample matrix $\{u_{ij}\}$ and the within-groups matrix $\{v_{ij}\}$, respectively; and $|U|$ and $|V|$ mean the determinants of matrixes $\{u_{ij}\}$ and $\{v_{ij}\}$, respectively. When Λ value is very large, clusters a and b cannot be cut, but must be merged into greater cluster c. By Rao's *F*-approximation, the *R*-statistic can be given by (Rao, 1965):

$$R = \frac{1-\Lambda^{1/S}}{\Lambda^{1/S}} \cdot \frac{Z \cdot S - P \cdot (K-1)/2 + 1}{P \cdot (K-1)} \tag{6a}$$

$$Z = n_h - 1 - (P+K)/2 \tag{6b}$$

$$S = \frac{P^2 \cdot (K-1)^2 - 4}{P^2 + (K-1)^2 - 5} \tag{6c}$$

where statistic R is distributed approximately as an *F*-variate with $v_1 = P \cdot (K-1)$and $v_2 = P \cdot (K-1)/2 + 1$ degrees of freedom. K is the number of groups, and P is the number of predictors. The *R*-statistics can reduce to an exact *F*-variate when $P = 1$ or 2, or when $K = 2$ or 3. Since the number of groups is two ($K = 2$) in this study, an exact *F* test is possible based on the Wilks' Λ criterion. Thus, we have $F(P, n_h - P - 1) = (1-\Lambda)/\Lambda \cdot (n_h - P - 1)/P$. The criteria of cutting and merging clusters become to make a number of *F*-tests (Rao, 1965). Second step is the tests of optimal cutting points. Sequence n_h samples in cluster h according to the values of $x_{r,i}^{(h)}$ in $\{x_i\}$ ($r = 1, 2, \ldots, n$). According to Wilks' likelihood ratio criterion, the optimal cutting point, which split the cluster h into two subclusters e and f when the samples are sequenced according to the values of $x_{r^*,i^*}^{(h)}$ in $\{x_{i^*}\}$, should satisfy that $\Lambda(n_e, n_f)$ is the minimum comparing to that of any other cutting alternatives. Then the *F* test can be undertaken. If

$$F(P', n_e - P' - 1) = \frac{1-\Lambda(n_e, n_f)}{\Lambda(n_e, n_f)} \cdot \frac{n_e - P' - 1}{P'} \geqslant F_1 \tag{7}$$

is satisfied, cluster h can then be cut into two subclusters e and f. x_{i^*} is identified as the most important predictor, which significantly affects the values of the predictands. Conversely, if Eq. (7) is not satisfied, cluster h cannot be cut. Then all the other clusters will be tested and cut if it satisfies the above testing criterion, until no cluster can be further cut. The next step is to test whether any two of the generated subclusters should be merged into a new cluster. For two clusters c and d among the existing H clusters, if

$$F(P', n_c + n_d - P' - 1) = \frac{1-\Lambda(n_c + n_d - 2, 1)}{\Lambda(n_c + n_d - 2, 1)} \cdot \frac{(n_c + n_d) - P' - 1}{P'} < F_2 \tag{8}$$

is satisfied, clusters c and d can be merged into a new cluster g. Otherwise, if Eq. (8) is not satisfied, clusters c and d cannot be merged. Then all the other clusters will be tested and merged if it satisfies the above testing criterion, until no clusters can be further merged. Final step is building a cluster tree for prediction. After all calculations and tests have been completed when all hypotheses of further cut or mergence are rejected, a cluster tree can be derived for a new sample prediction. The predictor values in the cluster tree will be used as the criteria to determine which end nodes the new predictor samples will enter into. The predictand values of the end nodes in the cluster tree will be used to calculate the values of the predictands corresponding to the new predictor samples. Each cutting point, which leads to two branches, corresponds to a value $x_{r^*,i^*}^{(h)}$ of the predictor x_{i^*}. When a new sample set of predictors $\{x_p\}$ is examined, its x_{p,i^*} values are compared with $x_{r^*,i^*}^{(h)}$ at the cutting points, and classified into relevant branches. Step-by-step, the sample finally enters into a tip branch (tip cluster) which cannot be either cut or merged further. Let e' be the tip branch where the new sample enters. Then, the predictands $\{y_p\}$ are:

$$y_p = y_p^{(e')} \pm R_p^{(e')} \tag{9}$$

where $y_p^{(e')}$ is mean of predictor y_p in sub-cluster e', and $R_p^{(e')}$ is radius of y_p in cluster e':

$$y_p^{(e')} = \frac{1}{n_{e'}} \sum_{k=1}^{n_{e'}} y_{p,k}^{(e')} \quad for all i \tag{10a}$$

$$R_p^{(e')} = \left\{ \max_{k=1}^{n_{e'}} (y_{p,k}^{(e')}) - \min_{k=1}^{n_{e'}} (y_{p,k}^{(e')}) \right\} / 2 \quad (10b)$$

Generally, based on the SCA technique, the daily climate-streamflow hydrological simulation can be developed (Zhuang et al., 2016b).

References

Andersson, L., Wilk, J., Todd, M.C., Hughes, D.A., Earle, A., Kniveton, D., Layberry, R., Savenije, H.H.G., 2006. Impact of climate change and development scenarios on flow patterns in the Okavango River. J. Hydrol. 331 (1–2), 43–57.

Borgomeo, E., Hall, J.W., Fung, F., Watts, G., Colquhoun, K., Lambert, C., 2014. Risk-based water resources planning: incorporating probabilistic nonstationary climate uncertainties. Water Resour. Res. 50, 6850–6873.

Charnes, A., Cooper, W.W., Kirby, P., 1972. Chance constrained programming: an extension of statistical method. In: Optimizing Methods in Statistics. Academic Press, New York, pp. 391–402.

Consigli, G., Dempster, M.A.H., 1998. Dynamic stochastic programming for asset-liability management. Ann. Oper. Res. 81, 131–161.

Deng, H.J., Chen, Y.N., Wang, H.J., Zhang, S.H., 2015. Climate change with elevation and its potential impact on water resources in the Tianshan Mountains, Central Asia. Global Planet. Change 76, 47–56.

Fan, Y.R., Huang, G.H., Li, Y.P., Kong, X.M., 2016. Bivariate hydrologic risk analysis based on coupled entropy-copula method for the Xiangxi River in Three Gorges Reservoir Area, China. Theor. Appl. Climatol. 125 (1), 381–397.

Gulpinar, N., Rustem, B., Settergren, R., 2002. Multistage stochastic programming in computational finance. In: Computational Methods in Decision Making, Economics and Finance: Optimization Models. Kluwer Academic Publishers, Dordrecht, pp. 33–45.

Harman, C.J., Troch, P.A., Sivapalan, M., 2011. Functional model of water balance variability at the catchment scale: 2. Elasticity of fast and slow runoff components to precipitation change in the continental United States. Water Resour. Res. 47, W02523.

Jiang, T., Chen, Y.D., Xu, C., Chen, X., Chen, X., Singh, V.P., 2007. Comparison of hydrological impacts of climate change simulated by six hydrological models in the Dongjiang Basin, South China. J. Hydrol. 336, 316–333.

Karamouz, M., Imen, S., Nazif, S., 2012. Development of a demand driven hydro-climatic model for drought planning. Water Resour. Manage. 26, 329–357.

Kandiah, V., Berglund, E., Binder, A., 2016. Cellular automata modeling framework for urban water reuse planning and management. J. Water Resour. Plan. Manage. 142 (12). https://doi.org/10.1061/(ASCE)WR.1943-5452.0000696. 04016054.

Kennedy, W.J., Gentle, J.E., 1981. Statistics: Textbooks and Monographs. Marcel Dekker, New York.

Kotir, J.H., Smith, C., Brown, G., Marshall, N., Johnstone, R., 2016. A system dynamics simulation model for sustainable water resources management and agricultural development in the Volta River Basin, Ghana. Sci. Total Environ. 573, 444–457.

Li, B.F., Chen, Y.N., Chen, Z.S., Xiong, H.G., Lian, L.S., 2016. Why does precipitation in northwest China show a significant increasing trend from 1960 to 2010? Atmos. Res. 167, 275–284.

Li, Y.P., Huang, G.H., Nie, S.L., 2006. An interval-parameter multi-stage stochastic programming model for water resources management under uncertainty. Adv. Water Resour. 29 (5), 776–789.

Li, Y.P., Huang, G.H., 2009. Fuzzy-stochastic-based violation analysis method for planning water resources management systems with uncertain information. Inf. Sci. 179, 4261–4276.

Li, Y.P., Huang, G.H., Huang, Y.F., Zhou, H.D., 2009a. A multistage fuzzy-stochastic programming model for supporting sustainable water resources allocation and management. Environ. Model. Softw. 24, 786–797.

Li, Z., Liu, W.Z., Zhang, X.C., Zheng, F.L., 2009b. Impacts of land use change and climate variability on hydrology in an agricultural catchment on the Loess Plateau of China. J. Hydrol. 377, 35–42.

Ling, H.B., Xu, H.L., Fu, J.Y., 2013. Temporal and spatial variation in regional climate and its impact on runoff in Xinjiang, China. Water Resour. Manage. 27, 381–399.

Lobell, D.B., Schlenker, W., Costa-Roberts, J., 2011. Climate trends and global crop production since 1980. Science 333, 616–620.

Loukas, A., Mylopoulos, N., Vasiliades, L., 2007. A modeling system for the evaluation of water resources management strategies in Thessaly, Greece. Water Resour. Manage. 21, 1673–1702.

Milly, P.C., Wetherald, R.T., Dunne, K.A., 2002. Increasing risk of great floods in a changing climate. Nature 415 (6871), 514.

Nash, J.E., Sutcliffe, J.V., 1970. River flow forecasting through conceptual models: Part I. A discussion of principles. J. Hydrol. 10, 282–290.

Naadimuthu, G., 1982. Stochastic modelling and optimization of water resources systems. Math. Model. 3 (2), 117–136.

Nguyen, H., Mehrotra, R., Sharma, A., 2016. Correcting for systematic biases in GCM simulations in the frequency domain. J. Hydrol. 538, 117–126.

Poulin, A., Brissette, F., Leconte, R., Arsenault, R., Malo, J.S., 2011. Uncertainty of hydrological modelling in climate change impact studies in a Canadian, snow-dominated river basin. J. Hydrol. 409, 626–636.

Poorsepahy-Samian, H., Espanmanesh, V., Zahraie, B., 2016. Improved inflow modeling in stochastic dual dynamic programming. J. Water Resour. Plan. Manage. 142 (12). https://doi.org/10.1061/(ASCE)WR.1943-5452.0000713. 04016065.

Rao, C.R., 1965. Linear Statistical Inference and its Applications. Wiley, New York.

Reshmidevi, T.V., Nagesh Kumar, D., Mehrotra, R., Sharma, A., 2018. Estimation of the climate change impact on a catchment water balance using an ensemble of GCMs. J. Hydrol. 556, 1192–1204. https://doi.org/10.1016/j.jhydrol.2017.02.016.

Rheinheimer, D., Null, S., Viers, J., 2016. Climate-adaptive water year typing for instream flow requirements in California's Sierra Nevada. J. Water Resour. Plan. Manage. 142 (11). https://doi.org/10.1061/(ASCE)WR.1943-5452.0000693, 04016049.

Risbey, J.S., 1998. Sensitivities of water supply planning decisions to streamflow and climate scenario uncertainties. Water Policy 1 (3), 321–340.

Sharma, A., Mehrotra, R., Johnson, F., 2012. A new framework for modelling future hydrologic extremes: nested bias correction as a precursor to stochastic rainfall downscaling. In: Surampalli, R.Y., Ojha, C.S.P. (Eds.), Green House Gas Emissions and Climate Change. American Society of Civil Engineers (ASCE), USA.

Sun, W., Huang, G.H., Lv, Y., Li, G.C., 2013. Inexact joint-probabilistic chance-constrained programming with left-hand-side randomness: an application to solid waste management. Eur. J. Oper. Res. 228, 217–225.

UNESCO, 2002. Coping with water scarcity. Technical Documents in Hydrology, No.58, Paris.

Wada, Y., Wisser, D., Eisner, S., Flörke, M., 2013. Multimodel projections and uncertainties of irrigation water demand under climate change. Geophys. Res. Lett. 40, 4626–4632.

Watkins, J., McKinney, D.C., Lasdon, L.S., Nielsen, S.S., Martin, Q.W., 2000. A scenario-based stochastic programming model for water supplies from the highland lakes. Int. Transit. Oper. Res. 7, 211–230.

Wang, X., Huang, G., Lin, Q., Nie, X., Cheng, G., Fan, Y., Li, Z., Yao, Y., Suo, M., 2013. A stepwise cluster analysis approach for downscaled climate projection – a Canadian case study. Environ. Model. Softw. 49, 141–151.

Wasko, C., Sharma, A., 2016. Continuous rainfall generation for a warmer climate using observed temperature sensitivities. J. Hydrol. 544, 575–590.

Wilby, R.L., Harris, I., 2006. A framework for assessing uncertainties in climate change impacts: low-flow scenarios for the river Thames, UK. Water Resour. Res. 42 (2), W02419.

Woldemeskel, F.M., Sharma, A., Sivakumar, B., Mehrotra, R., 2016. Quantification of precipitation and temperature uncertainties simulated by CMIP3 and CMIP5models. J. Geophys. Res. Atmos. 121, 3–17.

Xu, Z.X., Chen, Y.N., Li, J.Y., 2004. Impact of climate change on water resources in the Tarim River Basin. Water Resour. Manage. 18, 439–458.

Zarghami, M., Akbariyeh, S., 2012. System dynamics modeling for complex urban water systems: application to the city of Tabriz, Iran. Resour. Conserv. Recycl. 60, 99–106.

Zhuang, X.W., Li, Y.P., Huang, G.H., Liu, J., 2016a. Assessment of climate change impacts on watershed in cold-arid region: an integrated multi-GCM-based stochastic weather generator and stepwise cluster analysis method. Clim. Dyn. 47, 191–209.

Zhuang, X.W., Li, Y.P., Huang, G.H., Wang, X.Q., 2016b. A hybrid factorial stepwise-cluster analysis method for streamflow simulation – a case study in northwestern China. Hydrol. Sci. J. 61 (15), 2775–2788.